Distribution and Kinetics of Membrane Dielectric Polarization

II. Frequency Domain Studies of Gating Currents

JULIO M. FERNÁNDEZ, FRANCISCO BEZANILLA, and ROBERT E. TAYLOR

From the Department of Physiology, Ahmanson Laboratory of Neurobiology and Jerry Lewis Neuromuscular Research Center, University of California, Los Angeles, California 90024; The Laboratory of Biophysics, National Institute of Neurological and Communicative Disorders and Stroke, National Institutes of Health, Bethesda, Maryland 20205; and The Marine Biological Laboratory Woods Hole, Massachusetts 02543

ABSTRACT We have studied the admittance of the membrane of squid giant axon under voltage clamp in the absence of ionic conductances in the range of 0–12 kHz for membrane potentials (V) between −130 and 70 mV. The admittance was measured at various holding potentials (HP) or 155 ms after pulsing from a given holding potential. Standard P/4 procedure was used to study gating currents in the same axons. We found that the membrane capacity $C_m(\omega)$ is voltage as well as frequency dependent. For any given V, the voltage-dependent part of the membrane capacitance has a maximum as the frequency approaches zero and requires at least a two-time constant equivalent circuit to be described. When the holding potential is varied, the voltage-dependent capacitance follows a bell-shaped curve with a maximum change of 0.15 μF/cm^2 at about −60 mV. With the pulse method, the maximum is at −40 mV for HP = −70 and it shifts to −70 mV for HP = 0. The shift in the maximum of the voltage-dependent capacitance is consistent with the shift in the charge (Q) vs. V curve observed in our experiments with regular P/4 procedure when the HP is varied. Our data can be explained qualitatively by a four-state model for the sodium channel gating, where a charged particle can move within the field and interact with another particle not affected by the field.

INTRODUCTION

In 1952 Hodgkin and Huxley proposed that the mechanism for the coupling between the membrane conductance and membrane potential consisted of a field-dependent movement of charges that induced conformational changes in much larger units now called channels. Furthermore, this charge movement was postulated to be independent of the external chemical gradient and its movement was thought to be membrane bound. This general picture of the coupling between the electric field in the membrane and its conductance

J. GEN. PHYSIOL. © The Rockefeller University Press · 0022-1295/82/01/0041/27 $1.00 41
Volume 79 January 1982 41–67

makes some very precise predictions about the membrane dielectric properties; namely, a voltage-dependent polarization of the membrane that saturates outside the range of membrane potentials at which changes in conductance occur. Examination of these dielectric properties should prove useful in probing the molecular dynamics of channel opening and closing.

In 1973, Armstrong and Bezanilla measured a voltage-dependent asymmetry in the capacitive currents of squid giant axon membrane in response to large potential steps. The properties of this asymmetric current matched those expected from a saturable polarization, leading the authors to call them gating currents. Furthermore, Armstrong and Bezanilla (1975) showed that the capacitance measured with a transient method was voltage dependent and followed a bell-shaped curve. These measurements were also done by other authors (Keynes and Rojas, 1974; Meves, 1974) and in other preparations (Nonner et al., 1975). Much effort has been expended in obtaining a detailed description of gating currents (Keynes and Rojas, 1976; Armstrong and Bezanilla, 1974; Meves, 1974) and their relation to conductance changes in the membrane (Armstrong and Bezanilla, 1977; Armstrong and Gilly, 1979; Nonner, 1980).

A fundamental question remained. If the gating currents truly reflected the membrane-bound charge movement responsible for the opening and closing of the channels, it should be possible to detect a voltage-dependent admittance, measured with small signals, that would match the result of gating current measurements. Several authors attempted this approach (Fishman et al., 1977; Takashima, 1978), and their results did not agree with the expectations, raising the possibility that asymmetry currents might reflect other phenomena rather than a voltage-dependent, membrane-bound charge movement associated with gating.

In this paper we have studied the membrane capacitance under the same experimental conditions used to study gating currents. We found that the capacitance is voltage dependent and its properties can be compared to those measured in asymmetry current studies. We have also explored the source of our discrepancies with previous measurements of admittance and found that they can be explained when the long-term effects of depolarization are considered (Bezanilla et al., 1982).

The admittance method proves to be equivalent to time domain methods and it is especially useful in exploring the steady-state distribution of gating charges that cannot be conveniently studied with time domain methods.

A preliminary report of this work has been presented (Fernández et al., 1981).

METHODS

General

All our studies were performed on internally perfused voltage-clamped axons of *Loligo pealei* at the Marine Biological Laboratory, Woods Hole, Mass. Permeant cations were replaced by tetramethylammonium ion (TMA) and Tris-hydroximethyl amino methane (Tris) outside. As the external anion we have used either Cl^- or acetate, the latter

being used with the hope of reducing the amount of leakage current, which seems to have a small chloride component. The internal anion was always fluoride and glutamate.

Solutions are detailed in Table I of the preceding paper (Bezanilla et al., 1982). The acetate solution used in this study contained Ca acetate instead of $CaCl_2$. The convention followed is external solution//internal solution.

Experimental Chamber and Voltage-Clamp System

The voltage clamp and the perfusion chamber are identical to those described by Bezanilla et al. (1982), except that a provision to add two command voltages was incorporated in order to add a pseudo random binary sequence (PRBS) to a step of voltage (see Fig. 1).

Two outputs are available, $v(t)$ and $i(t)$, the measured membrane potential and current, respectively.

Command Signals

Three types of command signals can be applied to the voltage-clamp system: a PRBS, a pulse sequence, or a combination of the two (see Fig. 1).

The PRBS generator is the same as described by Clausen and Fernández (1981) and is based on a block diagram originally proposed by Poussart and Ganguly (1977). An important addition has been made. Instead of continually generating a periodic sequence, a sequence counter has been added such that a trigger pulse initiates the sequence generation but data acquisition is delayed by a programmable number of sequences. This allows for the necessary period of time needed to reach steady state in the measured response. We have found that usually a delay of one sequence is enough in any of the desired frequency ranges.

The PRBS generator provides a clock output that is used to synchronize the data acquisition. Exactly 1,024 clock pulses per sequence are generated after the programmed delay, as explained above. The maximum clock frequency is 26,392 kHz, giving a maximum effective bandwidth of 13.196 kHz, which can be divided to 6.598 or 3.229 kHz.

The amplitude of the PRBS can be varied continually but in all our experiments was fixed at 2 mV peak-to-peak.

The generator of pulse sequences has been described by Bezanilla et al. (1982). This pulse generator gives the trigger pulse to the PRBS generator such that for any given pulse pattern, the PRBS is locked in time with respect to the pattern.

Data Acquisition System

For data acquisition we used a combination module (DAS-250; Datel Intersil, Mansfield, Mass.) that consisted of a sample and hold, and a 12-bit analog-to-digital converter. The digital output of this module was fed to the memory of a Nova 3 minicomputer (Data General Inc., Southboro, Mass.), via data channel. The control signals of this module were provided by the computer under program control (Bezanilla et al., 1982) (see also Fig. 1.).

The signals fed to the data acquisition module (DAM) could come from two alternative pathways; for time domain measurements of gating currents, the current responses to a P/4 pulse pattern were subtracted from the signals produced by a transient generator (Fig. 1) in order to minimize the amplitude of the linear capacitive current (see Bezanilla and Armstrong, 1977). They were then fed to a variable gain amplifier and a six-pole Bessel low pass filter set at 30 or 50 kHz, after which the resulting signal was fed to the analog input of the DAM.

For frequency domain measurements, the current response to the PRBS was amplified with a variable gain amplifier and low pass filtered with a 120-dB/octave cour-elliptic filter, and finally fed to the DAM. All measurements presented here are the average of 16 cycles.

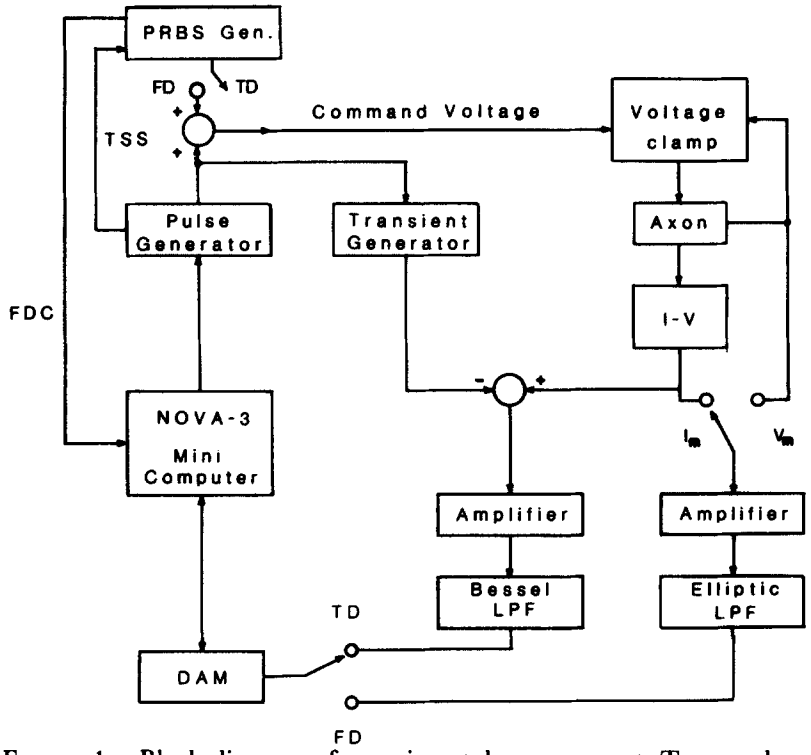

FIGURE 1. Block diagram of experimental arrangement. Two modes of operation are available: frequency domain (FD) and time domain (TD). For the FD mode, the command voltage is the sum of a pseudo random binary sequence (PRBS) and a pulse sequence generated by a pulse generator running under the control of the Nova 3 minicomputer. The pulse generator synchronizes the PRBS generator with the trigger start sequence pulse (TSS). Data acquisition into the computer through the data acquisition module (DAM) is synchronized by the frequency domain clock (FDC) generated by the PRBS generator. In this mode of operation, either the membrane potential v_m or the current i_m are amplified and fed to a cour-elliptic low pass filter (LPF) later being fed to the DAM. The time domain mode TD disables the PRBS generator, and makes use of a clock internally generated by the minicomputer, to synchronize the data acquisition. The membrane current in this mode, is amplified and applied to a six-pole Bessel LPF. Standard P/4 procedure is used in this mode (Bezanilla and Armstrong, 1977). The transient generator is coupled to the pulse generator and is used to increase the dynamic range of the input amplifier.

The change from one mode of operation to the other could be performed rapidly by simply disconnecting the PRBS input to the voltage clamp and switching the current output from one pathway to the other as indicated in Fig. 1. This feature allowed us to perform the two types of measurements in the same axons.

Computation of Admittance

To calculate the admittance of the membrane $Y_m(\omega)$, the membrane voltage $v(t)$ and the current response $i(t)$ were retrieved from the disk and Fourier transformed with a 1024 data point FFT (fast Fourier transform), the total measured admittance $Y(\omega) = I(\omega)/V(\omega) = G(\omega) + jB(\omega)$ is then numerically evaluated as follows:

$$Y(\omega) = \frac{X_{IV}(\omega)}{X_{VV}(\omega)}, \text{ with } X_{IV}(\omega) = \bar{V}(\omega)I(\omega);\ X_{VV}(\omega) = \bar{V}(\omega)V(\omega) \tag{1}$$

where $j = \sqrt{-1}$, and $\omega = 2\pi f$, where $V(\omega)$, $I(\omega)$ represent the Fourier transforms of $v(t)$ and $i(t)$, respectively, and the bar indicates a complex conjugate. The real and imaginary parts of the admittance $Y(\omega)$ correspond to conductance, $G(\omega)$, and susceptance, $B(\omega)$.

Series Resistance Compensation

To correct the admittance $Y(\omega)$ for the effects of the series resistance R_s, we applied the following procedure.

(*a*) The admittance obtained by the use of Eq. 1 was converted to impedance as:

$$Z(\omega) = R(\omega) + jX(\omega) = \frac{1}{Y(\omega)} = \frac{G(\omega)}{G^2(\omega) + B^2(\omega)} - j\frac{B(\omega)}{G^2(\omega) + B^2(\omega)}, \tag{2}$$

in which $R(\omega)$ and $X(\omega)$ are the resistance and reactance, respectively.

(*b*) To obtain the true membrane impedance, $Z_m(\omega)$, we only need to subtract R_s from the real part of $Z(\omega)$:

$$Z_m(\omega) = R(\omega) - R_s + jX(\omega). \tag{3}$$

(*c*) To obtain the corrected admittance, $Y_m(\omega)$, we reverse the first step as:

$$Y_m(\omega) = \frac{1}{Z_m(\omega)} = G_m(\omega) + jB_m(\omega) \tag{4}$$

where $G_m(\omega)$ is the membrane conductance and $B_m(\omega)$ is the membrane susceptance.

The estimates of the series resistance used in the procedure described above were calculated by measuring the initial voltage jump in response to a square pulse of current applied to the membrane (see Taylor et al., 1981, for references), giving values between 6 and 8 $\Omega \cdot cm^2$ for R_s when the external anion was chloride and values between 10 and 13 $\Omega \cdot cm^2$ when acetate was used instead of chloride. These values for R_s include the Schwann cell layer, connective tissue, and internal and external solutions. Our estimates for the contribution to R_s of the Schwann cell layer and connective tissue is between 2 and 3 $\Omega \cdot cm^2$, in good agreement with the values obtained by Salzberg et al. (1981).

In some cases, real time correction for R_s was done by the use of positive feedback in the voltage clamp (Hodgkin et al., 1952), in which a voltage, proportional to a fraction of the membrane current, is added to the measured membrane potential at the summing junction of the control amplifier. To calculate the admittance of the membrane with this correction, we have to use the uncorrected membrane potential $v(t)$ and the corrected current $i_m(t)$. This implies the assumption that the uncorrected $v(t)$ represents the membrane potential imposed across the membrane proper after correcting for R_s.

This method of correcting for R_s has the disadvantage of not being able to compensate for the full amount of R_s because of an increased instability of the voltage clamp.

Data Representation

Several representations of the admittance are used as defined below.

(*a*) Uncorrected conductance $G(\omega)$; uncorrected capacitance $C(\omega) = B(\omega)/\omega$.

(*b*) Membrane conductance $G_m(\omega)$; membrane capacitance $C_m(\omega) = B_m(\omega)/\omega$, where $G_m(\omega)$ and $B_m(\omega)$ are obtained after correcting $Y(\omega)$ for R_s as indicated in Eqs. 2–4.

(*c*) Nonlinear membrane conductance $G^n_m(\omega)$, and capacitance $C^n_m(\omega)$, obtained by subtracting from the membrane admittance obtained at a potential V, the membrane admittance measured at potential V_0 where $G_m(\omega)_{V0}$ and $C_m(\omega)_{V0}$ are voltage independent:

$$G^n_m(\omega)_V = G_m(\omega)_V - G_m(\omega)_{V0}$$

and

$$C^n_m(\omega)_V = C_m(\omega)_V - C_m(\omega)_{V0}$$

where the subscripts V and V_0 indicate the potential at which the admittance was measured.

(*d*) Complex capacitance $C^*_m(\omega) = C'_m(\omega) - jC''_m(\omega)$ where $C^*_m(\omega)$ can be calculated from the membrane admittance $Y_m(\omega)$ as:

$$C^*_m(\omega) = \frac{Y_m(\omega)}{j\omega} = \frac{B_m(\omega)}{\omega} + j\frac{G_m(\omega)}{\omega}.$$

The usual way to represent the complex capacitance is to plot $C''_m(\omega)$ vs. $C'_m(\omega)$. This diagram is usually referred to as a Cole-Cole plot in which $C'(\omega)$ represents the energy stored per cycle and $C''(\omega)$ represents the energy dissipated per cycle.

(*e*) Magnitude and phase angle of membrane admittance:

(*i*) uncorrected for leakage:

$$|Y_m(\omega)| = \sqrt{G^2_m(\omega) + B^2_m(\omega)},\ \phi_m(\omega) = \arctan\left(\frac{B_m(\omega)}{G_m(\omega)}\right);$$

(*ii*) corrected for leakage:

$$|Y^L_m(\omega)| = \sqrt{[G_m(\omega) - G_m(0)]^2 + B^2_m(\omega)},\ \phi^L_m(\omega) = \arctan\left(\frac{B_m(\omega)}{G_m(\omega) - G_m(0)}\right).$$

Smoothing and Fitting of Experimental Results

The raw data of capacity $C_m(\omega)$ and conductance $G_m(\omega)$ were usually smoothed with the recursive application of a triangular window described as:

$$x_i = \tfrac{1}{4}\, x_{i-1} + \tfrac{1}{2}\, x_i + \tfrac{1}{2}\, x_{i+1} \qquad i = 1, 2, \cdots n$$

in which x_i represents the $C_m(\omega)$ or $G_m(\omega)$ data points to be smoothed.

A wild-point editor was also used to delete the points due to the 60-Hz line interference and its harmonics. It consisted of averaging the two points adjacent to the one to be edited and substitution of this point by the result of the average.

To determine the validity and parameters of any given equivalent circuit of the membrane, we fitted this equivalent circuit to the experimental data by the use of a nonlinear least-square algorithm using the Levenberg-Marquardt method (Brown and Dennis, 1972).

Conductance $G_m(\omega)$ and capacitance $C_m(\omega)$ were simultaneously fitted. Each curve was normalized to its maximum value to weight the two plots equally.

RESULTS

We have measured the admittance $[Y(\omega)]$ between the voltage-measuring electrodes in a voltage-clamped axon perfused with impermeant ions. By definition, $Y(\omega) = G(\omega) + j\omega C(\omega)$. The conductance $[G(\omega)]$ and the capacitance $[C(\omega)]$ are shown in Fig. 2 *b* and *c* as functions of frequency for a number of different holding potentials. For comparison, the time domain gating currents recorded in the same axon are also shown in Fig. 2 *a* for several test pulses from a holding potential of −70 mV. The relation between the gating currrent in the time domain and the admittance in the frequency domain is by no means simple, as we shall discuss in more detail (see Discussion), but if the interpretation of the gating current as a time-dependent movement of charge confined to the membrane is correct, it is reasonable to expect that the admittance would represent a membrane with the properties of a voltage-dependent (saturable) lossy dielectric.

Fig. 2 *b* and *c* shows that the total membrane capacitance and conductance are frequency dependent as well as voltage dependent, having a maximum at a holding potential of −57 mV and decreasing for more depolarized or hyperpolarized potentials with the same asymptote in both cases. These characteristics are in excellent agreement with the expectation of a voltage-dependent, lossy dielectric.

To describe the voltage-dependent part of the membrane dielectric, which we associate with the gating currents, we must correct the total membrane admittance, $Y(\omega)$, for the effect of series resistance between the membrane and the voltage-measuring electrodes, to yield the true membrane admittance, $Y_m(\omega)$, which in turn needs to be corrected for any ionic leakage across the membrane. Only then does the resulting membrane admittance reflect the properties of the membrane dielectric. Finally, we must separate the voltage-dependent and voltage-independent parts of the corrected membrane admittance, $Y_m(\omega)$.

Correction for Series Resistance

As discussed in Methods, we have two ways to perform this correction, a real time correction by the use of negative resistance feedback in the voltage-clamp circuit or a numerical correction of the data performed by subtracting the estimated series resistance from the real part of the total impedance, $Z(\omega)$. The second method was applied routinely to our data, while the first one was applied in some experiments to check for the performance of our voltage clamp in the frequency range of our interest (0–12 kHz). Results for one case using both methods are shown in Fig. 3 *a* and *b* for capacitance and conductance at a holding potential of −70 mV. Trace number 1 is the uncorrected data, number 2 for correction using negative resistance compensation for 5.1 $\Omega \cdot cm^2$, and number 3 for numerical correction for 5.1 $\Omega \cdot cm^2$. Clearly, at <6 kHz the results are indistinguishable. At higher frequencies the agreement is

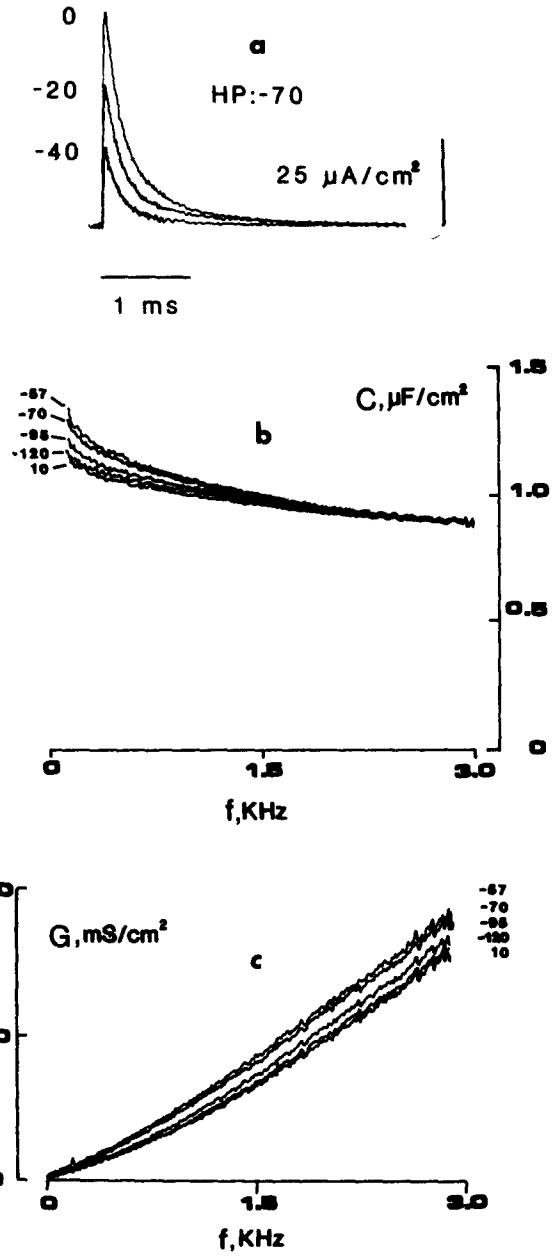

FIGURE 2. Two types of evidence for a voltage-dependent gating polarization in the membrane: (*a*) gating currents measured using standard P/4 procedure by giving test pulses from a holding potential of −70 mV. (*b*) and (*c*) show the capacitance and conductance, respectively, measured in steady state for different holding potentials. Tris-Cl-TTX//200 TMAFG (Bezanilla et al., 1982). Temperature, 7.5°C.

not as good. We interpret this as inadequacy of the negative resistance compensation, which is known to make the voltage clamp unstable.

The effect of the series resistance correction is significant and increases with frequency for both the capacitance and the conductance. For frequencies <500 Hz the correction is negligible. When the series resistance has been corrected for, the admittance, $Y_m(\omega)$, is the true admittance of the membrane and is equal to $G_m(\omega) + jB_m(\omega) = G_m(\omega) + j\omega C_m(\omega)$. At this stage, $G_m(\omega)$

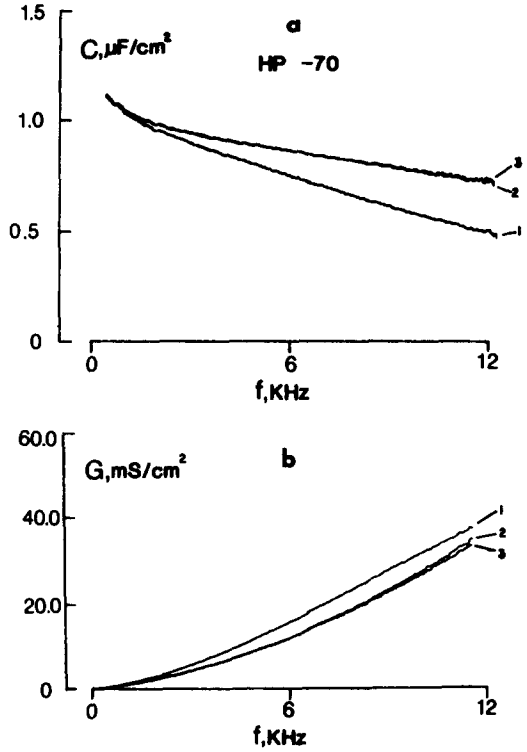

FIGURE 3. Series resistance correction: (*a*) and (*b*) show the capacitance and conductance measured at a holding potential of −70 mV; traces labeled 1 are the uncorrected data; traces labeled 2 and 3 have been corrected for 5.1 Ω·cm^2 by the use of the voltage-clamp series resistance compensation or numerical correction of the data, respectively. Tris-Cl-TTX//200 TMAFG. Temperature, 7.5°C.

is the sum of the leakage, and the apparent conductance contributed by the dielectric loss in the membrane. The capacitance $C_m(\omega)$ is a true measure of the real part of the complex capacitance. Any further results presented in this paper have been corrected for series resistance.

Correction for Leakage

In all of our experiments we have found nonlinear leakage, which in good axons can be of the order of 20 kΩ·cm^2 at 100 Hz at −70 mV. This leakage

increases in run-down axons and it also becomes time dependent, producing changes in the measured capacitance that are *not* a dielectric property of the membrane. Control experiments were performed at the beginning and end of a series of admittance measurements, and only those experiments in which the controls were superimposable have been considered.

Experiments in which the above criteria were fulfilled still showed in some cases a considerable voltage dependence of the low frequency conductance (5–15 $k\Omega \cdot cm^2$) with great variations in its magnitude from axon to axon. This clearly indicates the need to correct for the parallel leakage by separating the measured admittance into real and imaginary parts. This is the rationale for the use of the $G_m(\omega)$, $C_m(\omega)$ representation because after proper series resistance correction (see above) the non-time-dependent parallel leakage affects only the conductance. As the voltage-dependent and time-independent leakage does not appear in the imaginary part, the capacitance does not need leakage correction.

Fig. 4 shows $G_m(\omega)$ and $C_m(\omega)$ for two different holding potentials, +69 and −70 mV. A large increase in the leakage is observed when the membrane is held depolarized at +69 mV (Fig. 4 *c*). To correct for this leakage we simply subtract $G_m(\omega = 0)$ from $G_m(\omega)$ at +69 mV, obtaining the corrected conductance in Fig. 4 *d*. It is important to re-emphasize that this correction leaves the capacitance $C_m(\omega)$ unaffected (Fig. 4 *a* and *b*).

Voltage and Frequency-dependent Membrane Capacitance and Conductance

We have found (Taylor et al., 1981) that neither the conductance nor the capacitance varies significantly with holding potential for large hyperpolarizations or depolarizations (holding potential <-120 mV or $>+10$ mV) (see also Fig. 2 *b* and *c*). To separate the voltage-dependent part of the membrane admittance, we subtract $G_m(\omega)$ and $C_m(\omega)$ measured at large potentials from $G_m(\omega)$ and $C_m(\omega)$ measured at different holding potentials. The large potentials used were more positive than 10 mV or more negative than −120 mV.

The result of this subtraction procedure is shown in Fig. 5 *a* and *b*, and represents typical results from four experiments in which sufficiently depolarized or hyperpolarized potentials were reached without any noticeable deterioration of the axon. In this case the traces used for subtracting the voltage-independent admittance were obtained at +10 mV, where charge movement is nearly saturated (Bezanilla et al., 1982).

The simplest type of lossy dielectric can be described by a single capacitor in series with a resistance (we have subtracted the parallel capacitance) and is commonly referred to as a Debye type because he was the first to show that a molecular model could have this property. For any given Eyring type of model for charge translocation across the membrane, the resulting admittance could be represented by a linear combination of Debye type models. In the case of the data shown in Fig. 5 *a* and *b*, the solid lines represent $C_m^n(\omega)$ and $G_m^n(\omega)$ obtained by fitting two parallel Debye models where the time constants and their relative weights are voltage dependent and are listed in Table I.

For the data shown in Fig. 5 we found that for holding potentials of −95

and −120 mV, a single time constant model was sufficient, but for holding potentials of −70 mV and above, two time constants were required (see Table I). The fast time constant was largest (141 μs) for −70 mV and is in the same range as that found by Bezanilla and Taylor (1978) in the time domain. The slow time constant was also largest (1.45 ms) for a holding potential of −70 mV, which is somewhat larger than they found. It should be pointed out,

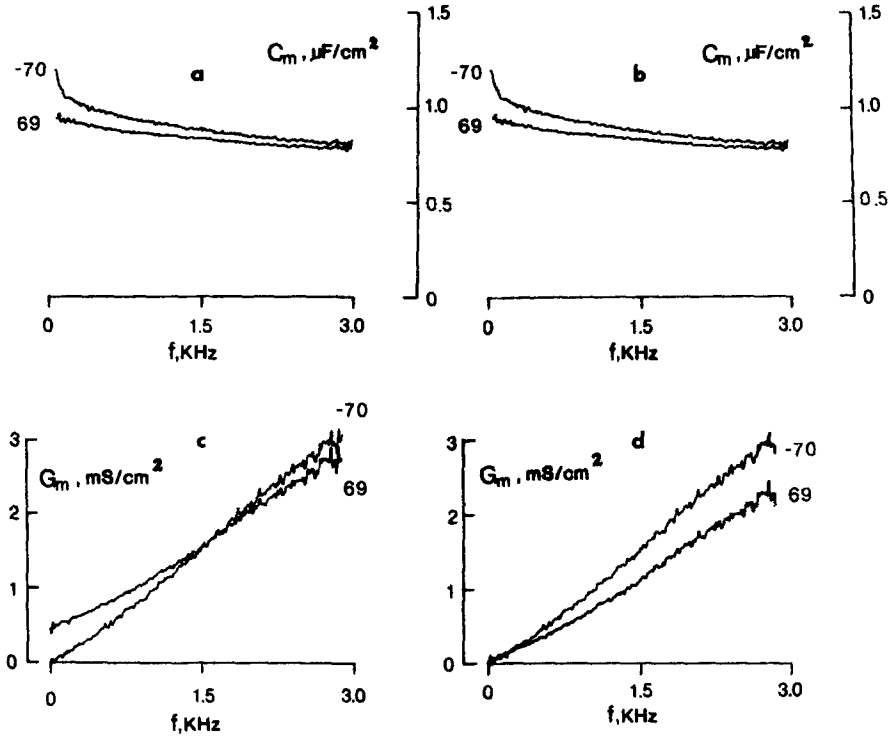

FIGURE 4. Leakage correction: (*a*) and (*c*) show capacitance and conductance, respectively, after correcting for series resistance, measured at 69 and −70 mV. The DC parallel leakage is of 20 kΩ·cm² for −70 mV and 2 kΩ·cm² for 69 mV as shown by the low frequency conductance. (*b*) and (*d*) show the effect of correcting for the parallel leakage of the data shown in (*a*) and (*c*). The leakage correction is performed by subtracting a constant, at all frequencies considered, from the data shown in (*c*), this constant corresponds to the conductance of the parallel leakage measured at each holding potential. Tris-Cl-TTX//200-TMAFG. Temperature, 12.5°C.

however, that with the present resolution, accurate determination of time constants larger than ~0.8 ms is not easy in the time domain. The sum of the capacitors in the equivalent circuit (Table I) would be the zero frequency capacitance if the model were adequate.

The maximum capacitance contributed by this voltage-dependent process at low frequencies (100 Hz) is in the range of 0.12–0.2 μF/cm² at about −57

mV. This value is less than previously expected on the basis of the time domain gating current measurements (see for example Taylor and Bezanilla, 1979). The main reason for this difference is now clear. It is simply that the maximum slope of the charge (Q) vs. V curve obtained by integration over a

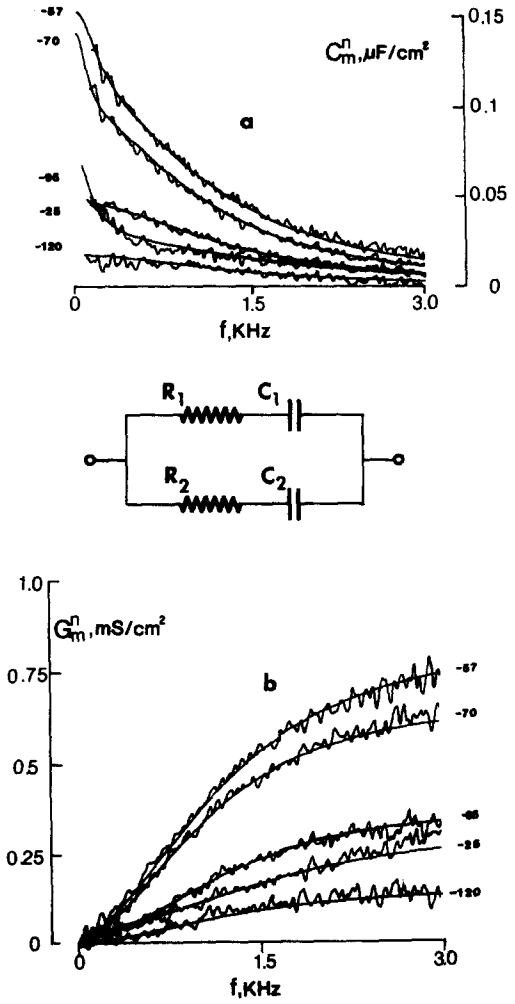

FIGURE 5. Membrane admittance after subtracting the voltage-independent part, obtained at 10 mV. This data corresponds to the total admittance shown in Fig. 2, after correction for series resistance. (*a*) and (*b*) show capacitance and conductance, respectively, at different holding potentials. The solid lines correspond to the two-time constant equivalent circuit (inset) fits of the admittance results. The parameters are listed in Table I.

certain period of time (2.5–5 ms) of the gating current does not necessarily occur at the holding potential (Bezanilla et al., 1982). We have measured some values for dQ/dV as measured from Q vs. V curves in the time domain at various holding potentials and found that the maximum values predicted

in this way are ~0.21 $\mu F/cm^2$, which is in good agreement with the apparent maximum change observed in the frequency domain. To make a direct comparison it is necessary that the period of time in which the displaced charge is integrated in the time domain is sufficient to include all the charge that moves at that potential and that the capacitance does not change below the frequency at which the comparison is made (see Discussion).

Measurements after a Potential Step

It has been shown that the general characteristics of the Q-V curves measured in the time domain when the integration period is ~2 ms are dependent upon the initial condition, except for the maximum charge that moves (Bezanilla et al., 1982). An example of this is the shift to more negative membrane potentials of the midpoint of the Q-V curve in the presence of inactivation. This predicts that the capacitance, as measured from the slope of the Q vs. V curves, would also be dependent on the initial conditions. It is important to realize that if

TABLE I

BEST FITS FOR R_1, R_2, C_1, AND C_2 FOR VARIOUS HOLDING POTENTIALS

HP	R_1	C_1	R_2	C_2	τ_1	τ_2
mV	$k\Omega \cdot cm^2$	$\mu F/cm^2$	$k\Omega \cdot cm^2$	$\mu F/cm^2$	μs	μs
−25	3.4	0.027	21.8	0.049	92	1,083
−57	1.24	0.10	14.0	0.053	124	742
−70	1.49	0.095	30.2	0.048	141	1,449
−95	2.58	0.048	—	—	123	—
−120	6.51	0.018	—	—	117	—

the measurements of charge movement in the time domain were performed for an infinite amount of time after stepping to a given test membrane potential, the total charge moved would correspond to the steady-state distribution of charges in the membrane and would be independent of the initial conditions. The same is true for the admittance measured with infinite frequency and range resolution.

If the total time required to make the admittance measurement is very small compared with changes in the system parameters, a quasi-steady state condition can be defined. This condition can be achieved by measuring admittance after a 155.2-ms delay from the onset of the pulse and for a total period of measurement of 155.2 ms, which corresponds to a 6.44-Hz frequency resolution in our 3,299.0-Hz bandwidth measurements. Under this condition, activation and fast inactivation processes are well over and slow inactivation has not yet developed.

Fig. 6 shows the membrane capacitance obtained under these conditions when pulsing to the indicated test membrane potential from a holding potential of 0 mV (record used to subtract linear capacitance was obtained by pulsing to +40 mV). Comparing these results for the voltage-dependent capacitance with those of Fig. 5 *a*, we see that during this quasi-steady state

the peak capacitance has shifted to −70 mV. There are also changes in the frequency dependence that we will not discuss in detail at this time.

Fig. 7 shows the voltage dependence of the capacitance measured at 100 Hz for various holding potentials (triangles) and for experiments performed under the quasi-steady state conditions described above, when giving test pulses from a holding potential of 0 mV (filled circles) or from −70 mV (squares) (these data correspond to three different axons). It can be seen that under

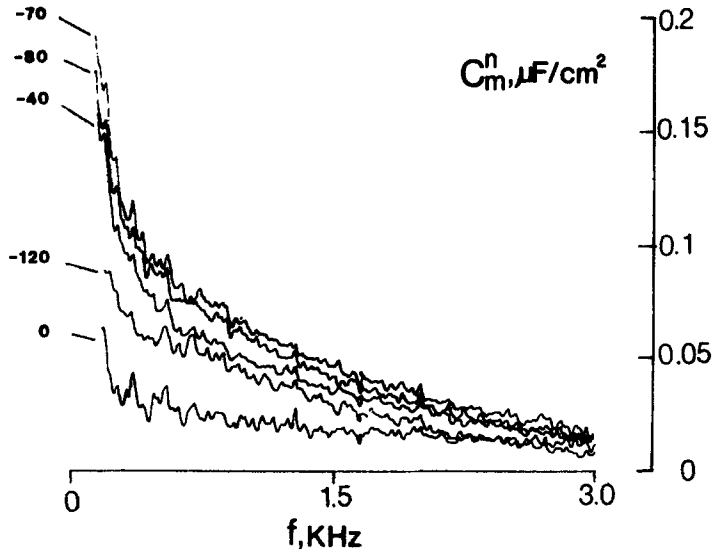

FIGURE 6. Voltage-dependent capacitance measured 155 ms after pulsing from a holding potential of 0 mV to the indicated potential. The record used to subtract the voltage-independent capacitance was obtained at 40 mV. Tris-Cl-TTX//200 TMAFG. Temperature, 12.5°C.

conditions where fast and slow inactivation are fully developed (holding at 0 mV), the peak capacitance occurs at −70 mV, but when they are removed the peak occurs at −40 mV (holding at −70 mV). The peak capacitance measured in steady-state conditions occurs at −57 mV. Fig. 7 shows that the capacitance can be modified by initial conditions when measured in a quasi-steady state and that these effects correspond qualitatively to the ones observed for the Q vs. V curves measured under similar conditions in the time domain.

However, a quantitative comparison cannot be made because there is no simple relation between the capacitance measured at 100 Hz and the measured slope of the Q vs. V curve under these conditions. A direct comparison can be made by the use of a model for the translocation of the gating particles across the membrane (see Discussion).

Complex Capacitance

As defined in Methods, the admittance of the membrane dielectric $[Y_m(\omega)]$ is equal to $j\omega C^*$ where $C^*(\omega) = C'_m(\omega) - jC''_m(\omega)$. A plot of $C''_m(\omega)$ vs. $C'_m(\omega)$

is often referred to as a Cole-Cole plot (see Cole and Cole, 1941). The plot for the non-voltage-dependent complex capacitance is discussed elsewhere (Taylor et al., 1981). They reported that for a holding potential of 0 mV the data from 10 Hz to 10 kHz fit rather well to an arc of a circle with center depressed below the real axis by 32.5° with intercepts on the real axis at 0.99 $\mu F/cm^2$ for zero frequency and 0.561 $\mu F/cm^2$ at infinite frequency with a maximum imaginary part at 12 kHz.

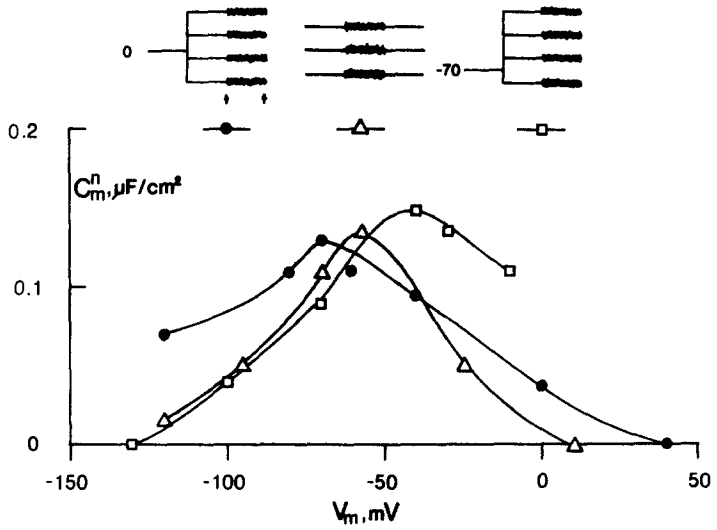

FIGURE 7. Voltage-dependent capacitance measured at f = 100 Hz as a function of membrane potential. The triangles correspond to measurements in steady state for various holding potentials. Tris-Cl-TTX//200 TMAFG. Temperature, 7.5°C. The filled circles correspond to measurements 155 ms after pulsing from a holding potential of 0 mV. Tris-Ac-TTX//200 TMAFG. Temperature, 12.5°C. Open squares correspond to measurements 155 ms after pulsing from a holding potential of −70 mV. Tris-Ac-TTX//200 TMAFG. Temperature, 12.5°C. The voltage-independent capacitance has been subtracted with records obtained at 10, 40, and −130 mV, respectively.

Fig. 8 is a Cole-Cole plot of the admittance obtained at −70 mV after vectorial subtraction of the voltage-independent part obtained at 69 mV. The solid line is derived from a two-time constant fit to the capacitance and conductance data, similar to that shown in Fig. 5 *a* and *b*.

DISCUSSION

Earlier attempts to show that the asymmetry currents observed in the time domain (gating currents) were associated with a voltage-dependent change in the membrane capacity did not give the expected result, raising an apparent paradox between measurements done in the time domain and in the frequency

domain. We have presented evidence showing that indeed the two approaches indicate a voltage-dependent capacity and we believe that the discrepancy with previous results can be explained by the methods used and unrealistic expectations.

As shown in Results, after a proper series resistance correction, a parallel leakage correction is necessary in order to represent the true membrane dielectric properties (a dielectric by definition has zero conductance at $\omega = 0$), which we can relate to the movement of gating charges.

As indicated previously, the presence of a significant amount of voltage-dependent leakage needs to be corrected for and this can be easily done if the data are represented as $G_m(\omega)$ and $C_m(\omega)$ as shown in Fig. 4. A very difficult problem arises if the data is represented as phase and magnitude because in this case the voltage-dependent leakage affects both and this makes it difficult to correct for and compare traces at different voltages. Fig. 9 shows the

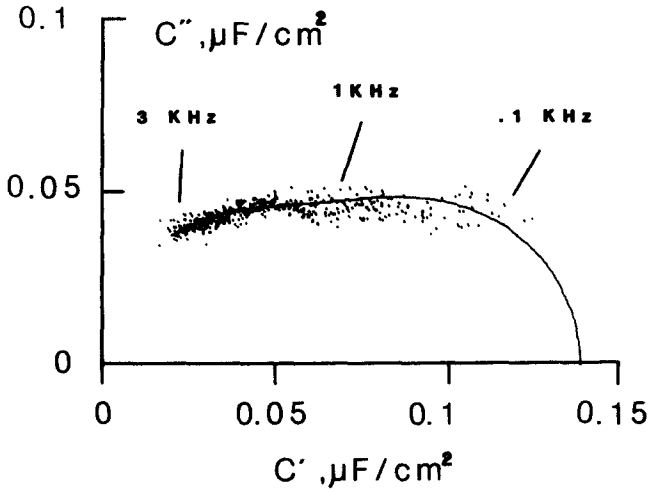

FIGURE 8. Cole-Cole plot of the voltage-dependent admittance. The voltage-independent part was subtracted from the admittance measured at a holding potential of −70 mV (record used for subtraction was obtained at 69 mV). The solid line corresponds to a two time constant fit of the voltage-dependent admittance. Tris-Cl-TTX//200 TMAFG. Temperature, 12.5°C.

magnitude and phase, calculated using the data from Fig. 4. The increase in leakage at +69 mV is evident in Fig. 9*a* and *c*: the magnitude tends to an asymptote at zero frequency and the phase angle tends to zero. If magnitude and phase are calculated after correcting for leakage by the procedure indicated above, then the effect of gating charge movement becomes readily apparent as is shown in Fig. 9*b* and *d*. In Fig. 9*b*, the magnitude of the corrected membrane admittance at +69 mV is consistently lower than the magnitude measured at −70 mV in the frequency range extending to 3,299 Hz. Similarly, in Fig. 9*d*, the phase angle of the corrected membrane admittance at +69 mV is higher in the whole range of 3,299 Hz than the value of

the phase angle measured at −70 mV. This is expected from a voltage-dependent capacitance and conductance with the characteristics shown in Fig. 4 *b* and *d*. It is apparent from these results that the magnitude and phase representation is inadequate in the presence of nonlinear leakage, which tends

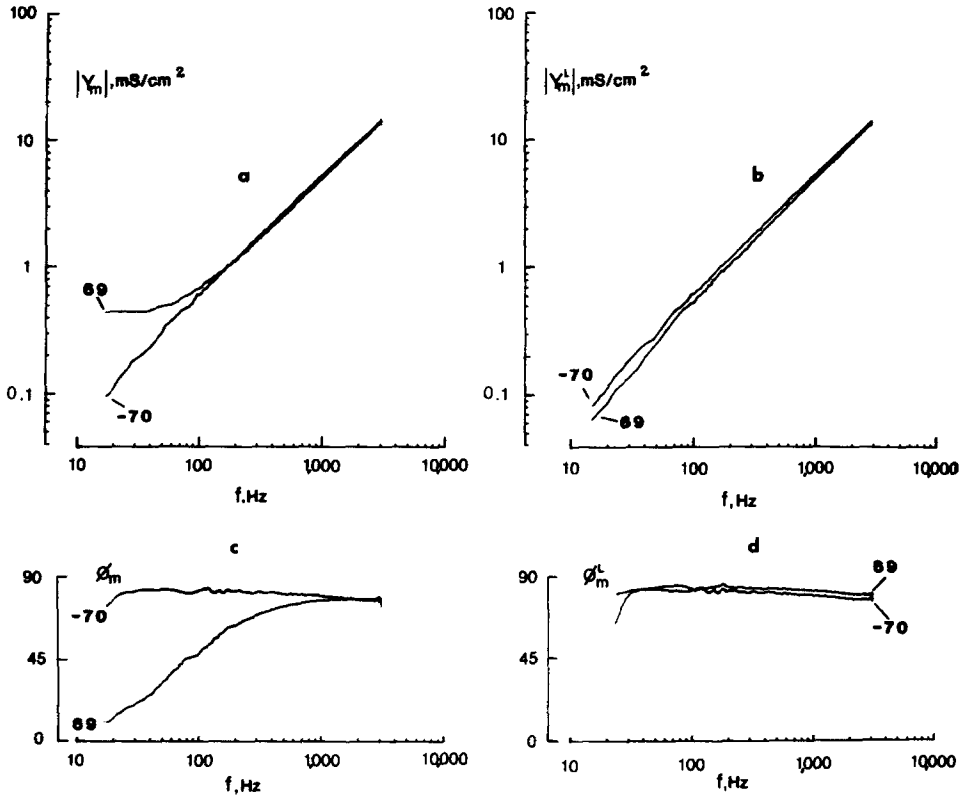

FIGURE 9. Effect of leakage on the magnitude and phase representation of the admittance data shown in Fig. 4: *a* and *c* show magnitude and phase of the admittance measured at holding potentials of 69 and −70 mV. If the leakage correction is performed as indicated in Fig. 4 and then the data are transformed into the magnitude and phase representation the effect of gating polarization becomes readily evident as shown in *b* and *d*.

to mask any change in capacitance in the frequency range in which gating can be observed. In fact, it may be noticed in Fig. 9 *a* that the values of the magnitudes at two different holding potentials cross each other and the capacitance change is very hard to recognize. Note, however, that the uncorrected capacitance shows an obvious change with holding potential. Fishman et al. (1977) presented results similar to the graphs shown in Fig. 9 *a* and *c* and they could detect a small capacitance decrease with depolarization consistent with the result of this paper.

The voltage-dependent part of the capacitance is also frequency dependent, as indicated by Taylor and Bezanilla (1979). This clarified the apparent

discrepancy with the results obtained by Takashima (1978), who measured capacitance at 1.5 kHz and had a standard deviation ~0.07 $\mu F/cm^2$. This large standard deviation would make it impossible to detect any voltage dependence in the capacity at that frequency (in 11 of our experiments the total change in capacity never reached 0.07 $\mu F/cm^2$ at 1.5 kHz).

Series Resistance

The series resistance can be a significant source of error. Its effect on the measured total capacitance $C(\omega)$ can be seen in Fig. 2*a* (compare curves 1 and 2, which correspond to $C(\omega)$ uncorrected and corrected for R_s, respectively). It is evident that R_s significantly alters the frequency dependence of $C(\omega)$ and that its effect grows rapidly with frequency.

It becomes evident, then, that in order to determine the lossy characteristics of both the voltage-dependent and voltage-independent (or linear) membrane capacitance $C_m(\omega)$, a correction for R_s is essential.

The effect of R_s on the voltage-dependent part of the membrane capacitance $C_m(\omega)$ can be seen by comparing Figs. 2*b* and 5*a*. Fig. 2*b* shows that the capacitance $C(\omega)$ is not voltage dependent near 3 kHz; however, if this datum is corrected for R_s, a significant voltage-dependent capacity $C_m(\omega)$ becomes apparent. Thus, any voltage-dependent dispersion occurring at frequencies >3 kHz would be masked out unless proper corrections for R_s are performed. In the time domain, the effects of R_s would be a significant change in the fast time constants of the gating currents, and it would also make any fast gating process difficult to observe. When there is significant series resistance, the rising phase of the time domain gating current will be distorted and it will appear not to be very voltage dependent.

An accurate description of gating currents requires series resistance correction. In the case of time domain measurements, the correction must be done in real time by the use of positive feedback (Hodgkin et al., 1952) because any posterior correction would be model dependent. A clear advantage of the frequency domain method is that the R_s correction can be done off line (see Methods), is model independent, and does not rely on the characteristics of the voltage clamp, which becomes unstable and noisy when full correction for R_s is attempted.

Ideally the series resistance should be measured in each axon with the highest possible accuracy. This is a difficult task because there is no unique way to determine it because of the loss in the membrane capacitance. Perhaps the most accurate determination of R_s is the one described by Salzberg et al. (1981), in which the true membrane potential is monitored with the use of potentiometric dyes.

Time and Frequency Domain Relationship

The most notorious features of the measurement of gating currents in the time domain are: (*a*) the charge displaced (Q) upon a sudden change of the membrane potential from a given holding potential to a variable V_m follows a sigmoidal curve that saturates at very hyperpolarized or depolarized poten-

tials. (*b*) The midpoint of the Q vs. V curve and its slope are dependent upon the initial conditions of the experiment (Bezanilla et al., 1982; Bezanilla and Taylor, 1979) related to fast and slow inactivation. The asymptotes of the Q vs. V curves are independent of the initial conditions, indicating that regardless of the experimental procedure, the total amount of gating charge available to move is always the same. (*c*) For any given potential and initial conditions, the measured gating currents can be described by at least two exponentials with their time constants as voltage-dependent parameters (Armstrong and Bezanilla, 1974).

The equivalent results in the frequency domain as described in this paper are: (*a*) for any given initial condition, the low-frequency capacitance follows a bell-shaped curve as a function of voltage as shown in Fig. 7. This is what is to be expected from a saturable ensemble of charges as indicated by the Q-V curves in the time domain. (*b*) We have also shown that the voltage at which C_m^n ($f = 100$) has its maximum depends on the initial conditions in very much the same way as the midpoint of the Q-V curves. (*c*) We have shown that the frequency dependence of the voltage-dependent capacitance can be described by at least the sum of two rational functions of the type (see Fig. 5):

$$C_m^n(\omega) = \frac{C_1}{1 + \omega^2\tau_1^2} + \frac{C_2}{1 + \omega^2\tau_2^2}$$

in which C_1, C_2, τ_1, and τ_2 are voltage dependent. This would correspond to two decaying exponentials in the time domain whose time constants are τ_1 and τ_2. The time constants measured in the frequency domain are listed in Table I, and their values are similar to the time constants measured in the time domain (Bezanilla and Taylor, 1978), but a quantitative comparison cannot be made because the experimental conditions are different.

A direct comparison between the results in time domain and frequency domain is difficult because it would require the measurement of gating currents in response to small pulses (2 mV amplitude). In theory, a direct comparison can be established between the zero frequency capacitance $C_m^n(0)$ and the slope of the Q-V at any given voltage. However, this requires integration of gating currents for infinite periods of time and an infinite frequency resolution in the frequency domain, which is clearly impossible. Another direct relation can be established between the time constants measured in the time and frequency domain, which, at any given voltage, regardless of the initial conditions, should be the same. However, the initial conditions change their relative weights, so a direct experimental comparison assumes that all the time constants in the time and frequency domain have been identified and that they can be measured regardless of their relative weights, which is also impossible experimentally.

In view of these difficulties we will attempt to establish the relation between time domain and frequency domain using a model based on a physical representation of the movement of groups in the membrane. The model was introduced in the previous paper (Bezanilla et al., 1982) and allows us to

predict results for the frequency and time domain properties that can be measured experimentally.

A Simple Physical Model for Charge Movement

We have used the simplest possible model for gating charge translocation across the membrane that can explain qualitatively the general features observed for the frequency and time domain measurements. This model (Bezanilla et al., 1982) is shown in Fig. 10*a*, and it is a kinetic representation of an activating particle that moves across the membrane and has the function of opening the Na^+ channel and an inactivating particle that moves perpendicular to the field with rate constants π and ϵ that are voltage independent. The two particles interact in the closed state (1) with an interaction energy W_0 (in kT units), the other states being open (2), closed-inactivated (4), and open-inactivated (3). The time constant of inactivation is very large (>10 s) and corresponds to slow inactivation (Bezanilla et al., 1982). If the time that it takes to make any of the measurements either in time or frequency domain is short compared with the inactivation time constant, a further simplification of the model can be performed. In this case we can consider that during the measurement

$$Q_1 + Q_2 = Q'_T$$

and

$$Q_3 + Q_4 = Q''_T$$

in which Q'_T and Q''_T are constants determined by the initial conditions, which are presumed to represent a true equilibrium of charges (see Appendix 1). Under these conditions the system is reduced to two parallel reactions that correspond to the opening of the channel with and without inactivation.

Fig. 10*b–d* show the predicted results in the time and frequency domain. Fig. 10*b* shows $Q = Q_2 + Q_3$ (which corresponds to the charge translocated) as a function of the test voltage for two different initial conditions: HP = 0 and HP = −70 mV. Each Q-V curve is the sum of two; one corresponds to the translocation from 1 to 2 and the other to the translocation between 4 and 3. These two Q vs. V curves have their center points shifted with respect to the other, and the amount of the shift is independent of the initial conditions, depending only on the parameters used in the model.

Since the weight of each of these partial Q-V curves depends on the amount of charge in each state, which in turn depends on the initial conditions, the Q vs. V curve resulting from the sum of the two will have its centerpoint shifted in the direction of the one that carries more weight, as discussed in the previous paper (Bezanilla et al., 1982), in connection with fast and slow inactivation.

This model also predicts that the voltage at which the low-frequency capacitance has its peak is dependent on the initial conditions, being again the sum of the two C-V curves whose weights are dependent on initial conditions, as shown in Fig. 10*d*. In the same graph we have also plotted the

predicted steady-state low-frequency capacitance as a function of holding potential, which has its peak between the *C-V* curves for holding at −70 and 0 mV. The relative amplitudes of the maximum capacitative change for the various initial conditions as shown in Fig. 10*d* cannot be compared directly to

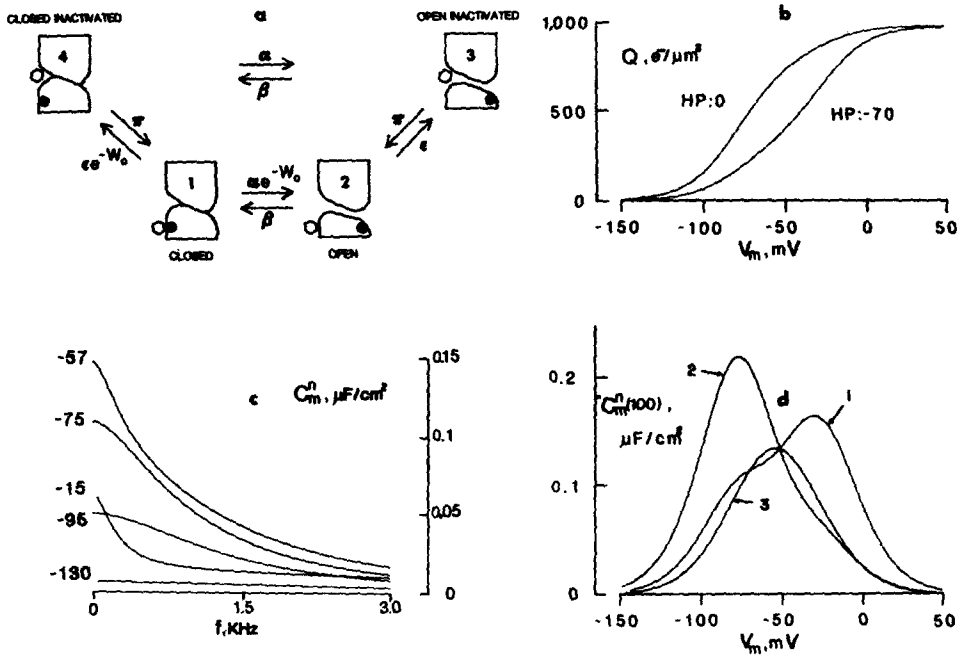

FIGURE 10. Time and frequency domain predictions of a four-state model for Na^+ channel gating. (*a*) shows the model where the labels 1, 2, 3, and 4 indicate the channel closed, open, open-inactivated, and closed-inactivated. The values used in the parameters are: $W_0 = 3.3$, $W_1 = 23.7$, $W_2 = 18.6$, $W_3 = 32.3$, $W_4 = 33.9$, and $z = 1.6$ where W_0 is the interaction energy between the activating and inactivating particles, and W_1, W_2, W_3, and W_4, correspond to the activation energies of α, β, ϵ, π, respectively, all expressed in kT units. Total charge density is considered to be 1,000 $e^-/\mu m^2$. (*b*) shows total charge displaced into states 2 and 3 as a function of potential for two given initial conditions: HP = 0 mV, HP = −70 mV. (*d*) shows the prediction for C_m^n (f = 100 Hz) when measured 155.2 ms after pulsing from a holding potential of −70 mV (1) or 0 mV (2). Trace number 3 corresponds to the predicted values of C_m^n (f = 100 Hz) when measured in steady state as a function of the holding potential. (*c*) corresponds to the frequency dependence of the capacitance for various holding potentials.

the data of Fig. 7, which correspond to different axons. Small errors in the estimates of the total area in each axon plus the fact that the subtraction of the linear capacitance has been performed at different potentials for each case could easily account for the observed differences in the relative amplitudes.

It is also of interest to consider the frequency dependence of the voltage-dependent capacitance to compare with the experimental results. This has

been done for the capacitance as a function of holding potential in Fig. 10*c* using the same parameters used in Fig. 10*b* and *d*. The detailed procedure of this calculation is shown in the Appendix.

This simple four-state model shows most of the features of the *Q-V* curves and *C-V* curves as a function of holding potentials. Experiments done with prepulses to separate fast and slow inactivation, as shown in the previous paper, have not been done in the frequency domain because the time it takes to do the measurement is usually longer than the relaxation times of fast inactivation. As was shown in the previous paper, when results of short-term depolarization are compared with prolonged depolarization, we need to consider two separate processes that lead us to a model containing eight states. Consequently, the present version of the four-state model can be considered the lumped effects of both short-term and long-term voltage conditioning.

It is clear that the measurements done in the frequency and in the time domain and correlated with the help of the four-state model are consistent with the interpretation that gating currents are the movement of a group of charges bound to the membrane exhibiting voltage dependence and saturation. These charges are the basis of a voltage-dependent, frequency-dependent lossy capacitance and they are connected with the conformational changes that activate and inactivate the sodium conductance.

APPENDIX

Charge Movement and Admittance of the Four-State Model

Throughout our calculations, all energies W_i, i = 0, 1, 2, 3, 4 are expressed in kT units and the rate constants α, β, π, ϵ are in s^{-1}. The model considered is the one shown in Fig. 10*a*.

The total amount of charge available to move is labeled as Q_T; then

$$\sum_{i=1}^{4} Q_i = Q_T;$$

the indices are defined as 1, closed; 2, open; 3 open-inactivated; and 4, closed-inactivated.

The barriers are considered symmetrical (peak located at one half of the electrical distance) and are defined as

$$\alpha = \frac{kT}{h}\exp - \left(W_1 - \frac{ezV}{2kT}\right), \qquad \beta = \frac{kT}{h}\exp - \left(W_2 + \frac{ezV}{2kT}\right)$$

where W_1 and W_2 are the heights of the respective barriers of the activating particle that translocates across the membrane, e is the electronic charge in coulombs, z is the valence, and V is the membrane voltage defined as the potential inside minus the potential outside of the axon membrane. T is absolute temperature and k and h are Boltzmann and Planck constants, respectively.

$$\epsilon = \frac{kT}{h}\exp(-W_3)$$

$$\pi = \frac{kT}{h}\exp(-W_4)$$

where W_3 and W_4 correspond to the heights of the barrier for the inactivating particle. W_0 is the energy of interaction between the activating and inactivating particles. The polarization current is given by

$$I_g = \frac{dQ_2}{dt} + \frac{dQ_3}{dt} = F_g(Q_2, Q_3, V). \tag{A1}$$

Linearizing F_g and then taking the Laplace transform of the resulting equations, one obtains

$$\delta\tilde{I}_g = \left(\frac{\partial F_g}{\partial Q_2}\right)_p \delta\tilde{Q}_2 + \left(\frac{\partial F_g}{\partial Q_3}\right)_p \delta\tilde{Q}_3 + \left(\frac{\partial F_g}{\partial V}\right)_p \delta\tilde{V} \tag{A2}$$

where the symbol ~ indicates a transformed variable. p represents the operating point.

The admittance can be calculated as

$$Y_m^n(\omega) = \frac{\delta\tilde{I}_g}{\delta\tilde{V}}. \tag{A3}$$

The partials of F_g; $\left(\frac{\partial F_g}{\partial Q_2}\right)_p$, $\left(\frac{\partial F_g}{\partial Q_3}\right)_p$, $\left(\frac{\partial F_g}{\partial V}\right)_p$ can be determined directly from Eq. A1 and then evaluated at the operating point with Q_{2p}, Q_{3p}, V_p, which are calculated using the equilibrium equations and the specified V_p.

The remaining terms of Eq. A3, $\frac{\delta\tilde{Q}_2}{\delta\tilde{V}}, \frac{\delta\tilde{Q}_3}{\delta\tilde{V}}$ need to be evaluated as follows:

if

$$\begin{aligned}
\frac{dQ_1}{dt} &= F_1(Q_1, Q_2, Q_3, V) \\
\frac{dQ_2}{dt} &= F_2(Q_1, Q_2, Q_3, V) \\
\frac{dQ_3}{dt} &= F_3(Q_1, Q_2, Q_3, V)
\end{aligned} \tag{A4}$$

then by linearizing this system of equations and then Laplace transforming it, one obtains a system of equations

$$\begin{aligned}
\left(\frac{\partial F_1}{\partial V}\right)_p &= \frac{\delta\tilde{Q}_1}{\delta\tilde{V}}\left[\left(\frac{\partial F_1}{\partial Q_1}\right)_p - s\right] + \frac{\delta\tilde{Q}_2}{\delta\tilde{V}}\left(\frac{\partial F_1}{\partial Q_2}\right)_p + \frac{\delta\tilde{Q}_3}{\delta\tilde{V}}\left(\frac{\partial F_1}{\partial Q_3}\right)_p \\
\left(\frac{\partial F_2}{\partial V}\right)_p &= \frac{\delta\tilde{Q}_1}{\delta\tilde{V}}\left(\frac{\partial F_2}{\partial Q_1}\right)_p + \frac{\partial\tilde{Q}_2}{\delta\tilde{V}}\left[\left(\frac{\partial F_2}{\partial Q_2}\right)_p - s\right] + \frac{\delta\tilde{Q}_3}{\delta\tilde{V}}\left(\frac{\partial F_2}{\partial Q_3}\right)_p \\
\left(\frac{\partial F_3}{\partial V}\right)_p &= \frac{\delta\tilde{Q}_1}{\delta\tilde{V}}\left(\frac{\partial F_3}{\partial Q_1}\right)_p + \frac{\delta\tilde{Q}_2}{\delta\tilde{V}}\left(\frac{\partial F_3}{\partial Q_2}\right)_p + \frac{\delta\tilde{Q}_3}{\delta\tilde{V}}\left[\left(\frac{\partial F_3}{\partial Q_3}\right)_p - s\right]
\end{aligned} \tag{A5}$$

where the partials can be directly evaluated from Eq. A4 and s is the Laplace transform variable. This system of equations needs to be solved for $\frac{\delta\tilde{Q}_2}{\delta\tilde{V}}$ and $\frac{\delta\tilde{Q}_3}{\delta\tilde{V}}$,

giving

$$\frac{\delta \tilde{Q}_2}{\delta \tilde{V}} = \frac{B_1(x_1 + s)(x_2 + s)}{(z_1 + s)(z_2 + s)(z_3 + s)}, \qquad \frac{\delta \tilde{Q}_2}{\delta \tilde{V}} = \frac{B_2(y_1 + s)(y_2 + s)}{(z_1 + s)(z_2 + s)(z_3 + s)} \tag{A6}$$

where B_1 and B_2 are constants, and x, y, and z are the zeroes of the determinants evaluated for $\frac{\delta \tilde{Q}_2}{\delta \tilde{V}}, \frac{\delta \tilde{Q}_3}{\delta \tilde{V}}$ and the homogeneous determinant, respectively. Replacing (A6) in (A3) we calculate the admittance as

$$Y_m^n(\omega) = \left(\frac{\partial F_g}{\delta Q_2}\right)_p \frac{B_1(x_1 + s)(x_2 + s)}{(z_1 + s)(z_2 + s)(z_3 + s)} + \left(\frac{\partial F_g}{\partial Q_3}\right)_p \frac{B_2(y_1 + s)(y_2 + s)}{(z_1 + s)(z_2 + s)(z_3 + s)} + \left(\frac{\partial F_g}{\partial V}\right)_p. \tag{A7}$$

The admittance can be separated in real and imaginary parts by substituting $s = j\omega$, giving a result in the form

$$Y_m^n(\omega) = G_m^n(\omega) + j\omega C_m^n(\omega).$$

The capacitance $C_m^n(\omega)$ predicted in this way, by using the kinetic model shown in Fig. 10*a*, is voltage dependent and its frequency dependence has three time constants, z_1, z_2, and z_3.

Two Time Constant Approximation

As discussed previously, if the rate constants π and ϵ are made small enough (close to the rate constant for slow inactivation) and the measurements are performed in a period of time that is small compared with this time constant, then during the time of the measurement the system is in quasi-steady state. This allows us to predict the admittance measured in the pulse experiments (see Figs. 6 and 7) with the following procedure.

For any given holding potential the distribution of Q_T in each of the states is calculated from the equilibrium equations giving

$$Q_1 + Q_2 = Q'_T$$
$$Q_3 + Q_4 = Q''_T,$$

where $$Q'_T + Q''_T = Q_T$$

and it is then assumed that Q'_T and Q''_T remain constant during the measurements, with the pulse procedure of charge movement in time domain or admittance in frequency domain.

This assumption allows us to treat the four-state model of Fig. 10*a* as two two-state models functioning in parallel, each with a total amount of charge available to move Q'_T and Q''_T, respectively, which is determined by the initial conditions as:

$$Q''_T = \frac{Q_T(1 + \alpha/\beta)}{1 + \frac{\epsilon}{\pi e^{-W_o}} + \frac{\beta}{\alpha}\left(1 + \frac{\epsilon}{\pi}\right)} \tag{A8}$$

and $$Q'_T = Q_T - Q''_T$$

where the rate constants as previously defined are evaluated for the given holding potential.

The charge movement measured in the time domain in a short period of time is then given by the "equilibrium" distribution of Q'_T and Q''_T in states 2 and 3, respectively, evaluated at the potential of the pulse.

The admittance can be calculated using the procedure described above, for each of the two-state models, and since they are in parallel, the total admittance is simply the sum of the two.

The predicted admittance is given by

$$Y_m^n(j\omega) = \left(\frac{\partial F_2}{\partial V}\right)_p \left(\frac{s}{s - \left(\frac{\partial F_2}{\partial Q_2}\right)_p}\right) + \left(\frac{\partial F_3}{\partial V}\right)_p \left(\frac{s}{s - \left(\frac{\partial F_3}{\partial Q_3}\right)_p}\right) \tag{A9}$$

where

$$F_2 = \frac{dQ_2}{dt}, \qquad F_3 = \frac{dQ_3}{dt}$$

and the partials are evaluated at the operating point p which corresponds to the membrane voltage attained by the pulse.

The admittance evaluated in Eq. A9 can be separated in real and imaginary parts as

$$Y_m^n(\omega) = G_m^n(\omega) + j\omega C_m^n(\omega)$$

where $C_m^n(\omega)$ is given by

$$C_m^n(\omega) = \frac{C_2}{1 + \omega^2\tau_2^2} + \frac{C_3}{1 + \omega^2\tau_3^2}$$

with

$$C_i = -\frac{\left(\frac{\partial F_i}{\partial V}\right)_p}{\left(\frac{\partial F_i}{\partial Q_i}\right)},$$

$$\tau_i = -\frac{1}{\left(\frac{\partial F_i}{\partial Q_i}\right)_p}, \qquad i = 2, 3.$$

Supported by grants AM25201 and GM30376 from the U. S. Public Health Service, the Muscular Dystrophy Association, and Du Pont de Nemours and Co.

Received for publication 16 April 1981 and in revised form 26 August 1981.

REFERENCES

ARMSTRONG, C. M., and F. BEZANILLA. 1973. Currents related to movement of the gating particles of the sodium channels. *Nature* (*Lond.*). **242:**459–461.

ARMSTRONG, C. M., and F. BEZANILLA. 1974. Charge movement associated with the opening and closing of the activation gates of the Na channels. *J. Gen. Physiol.* **63:**533–552.

ARMSTRONG, C. M., and F. BEZANILLA. 1975. Current associated with the ionic gating structures in nerve membranes. *Ann. N. Y. Acad. Sci.* **274:**265–277.

ARMSTRONG, C. M., and F. BEZANILLA. 1977. Inactivation of the sodium channel. II. Gating current experiments. *J. Gen. Physiol.* **70:**567–590.

ARMSTRONG, C. M., and W. F. GILLY. 1979. Fast and slow steps in the activation of sodium channels. *J. Gen. Physiol.* **74:**691–711.

BEZANILLA, F., and R. E. TAYLOR. 1979. Effects of holding potential on gating currents in the squid giant axon. *Biophys. J.* **25:**193*a*.

BEZANILLA, F., R. E. TAYLOR, and J. M. FERNÁNDEZ. 1982. Distribution and kinetics of membrane dielectric polarization. I. Long-term inactivation of gating currents. *J. Gen. Physiol.* **79:**21–40.

BROWN, K. M., and J. E. DENNIS. 1972. Derivative free analogues of the Levenberg-Marquardt and Gauss algorithms for non-linear least squares approximations. *Numerische Mathematik.* **8:** 289–297.

CLAUSEN, C., and J. M. FERNÁNDEZ. 1981. A low cost method for rapid transfer function measurements with direct application to biological impedance analysis. *Pflugers Archiv.* **390:** 290–295.

COLE, K. S., and R. H. COLE. 1941. Dispersion and absorption in dielectrics. I. Alternating current characteristic. *J. Chem. Phys.* **9:**341–351.

FERNANDEZ, J. M., R. E. TAYLOR, and F. BEZANILLA. 1981. Gating currents in the frequency domain. *Biophys. J.* **33:**281*a*.

FISHMAN, H. M., L. E. MOORE, and D. POUSSART. 1977. Asymmetry currents and admittance in squid axons. *Biophys. J.* **19:**177–183.

HODGKIN, A. L., and A. F. HUXLEY. 1952. A quantitative description of membrane current and its application to conduction and excitation in nerve. *J. Physiol.* (*Lond.*). **117:**500–544.

HODGKIN, A. L., A. F. HUXLEY, and B. KATZ. 1952. Measurements of current-voltage relations in the membrane of the giant axon of *Loligo*. *J. Physiol.* (*Lond.*). **116:**424–448.

KEYNES, R. D., and E. ROJAS. 1974. Kinetics and steady state properties of the charged system controlling sodium conductance in the squid giant axon. *J. Physiol.* (*Lond.*). **233:**28–30P.

KEYNES, R. D., and E. ROJAS. 1976. The temporal and steady state relationship between activation of the sodium conductance and movement of the gating particles in the squid giant axon *J. Physiol.* (*Lond.*). **255:**157–189.

MEVES, H. 1974. The effect of holding potential on assymetry current in squid giant axons. *J. Physiol.* (*Lond.*). **243:**847–867.

NONNER, W. 1980. Relations between the inactivation of sodium channels and immobilization of gating charge in frog myelinated nerve. *J. Physiol.* (*Lond.*). **299:**573–603.

NONNER, W., E. ROJAS, and R. STAMPFLI. 1975. Gating currents in the node of Ranvier: voltage and time dependence. *Philos. Trans. R. Soc. Lond. B Biol. Sci.* **270:**483–492.

POUSSART, D., and U. S. GANGULY. 1977. Rapid measurement of system kinetics: an instrument for real time transfer function analysis. *Proc. IEEE.* **65:741–747.**

SALZBERG, B. M., F. BEZANILLA, and H. V. DAVILA. 1981. An optical determination of the series resistance in giant axons of *Loligo pealei*. *Biophys. J.* **33:**90*a*.

TAKASHIMA, S. 1978. Frequency domain analysis of asymmetry current in squid axon membrane. *Biophys. J.* **22:**115–119.

TAYLOR, R. E., and F. BEZANILLA. 1979. Comments on the measurement of gating currents in the frequency domain. *Biophys. J.* **26:**338–340.

TAYLOR, R. E., J. M. FERNANDEZ, and F. BEZANILLA. Squid axon membrane low frequency diectric properties. *In* "The Biophysical Approach to Excitable Systems. Proceedings of Symposium honoring Kenneth S. Cole on his 80th birthday. Adelman and Goldman, editors. Plenum Press Publ. Co., New York. In press.